Proceedings of the ASME Turbo Expo 2024
Turbomachinery Technical Conference and Exposition
GT2024
June 24-28, 2024, London, United Kingdom

GT2024-125834

PREDICTION OF SOOT IN AN RQL BURNER USING A SEMI-DETAILED JETA-1 CHEMISTRY

Etienne Lameloise[1], Bénédicte Cuenot[1], Eleonore Riber[1,*], Aurélien Perrier[2], Gilles Cabot[2], Frédéric Grisch[2]

[1]Centre Européen de Recherche et de Formation Avancée au Calcul Scientifique (CERFACS), Toulouse, France
[2]Normandie Univ., UNIROUEN, INSA Rouen Normandie, CNRS, CORIA, 76000 Rouen, France

ABSTRACT

The present work proposes a methodology to include accurate kinetics for soot modeling taking into account real fuel complexity in Large Eddy Simulation (LES) of aeronautical engines at a reasonable computational cost. The methodology is based on the construction of an analytically reduced kinetic mechanism describing both combustion and gaseous soot precursors growth with sufficient accuracy on selected target properties. This is achieved in several steps, starting from the selection of the detailed kinetic model for combustion and soot precursors growth, followed by the determination of a fuel surrogate model describing the complex real fuel blend. Finally the selected kinetic model is analytically reduced with the code ARCANE while controlling the error on flame properties and soot prediction for the considered fuel surrogate. To perform all evaluation and reduction tests on canonical sooting flames, a Discrete Sectional Model (DSM) for soot has been implemented in Cantera. The resulting code (Cantera-soot) is now available for the fast calculation of soot production in laminar flames for any fuel. The obtained reduced kinetic scheme is finally validated in a Rich-Quench-Lean (RQL) burner of the literature in terms of soot prediction capabilities by comparison of LES coupled to the Lagrangian Soot Tracking model (LST) with measurements. Results show a significant improvement of the soot level prediction when using the reduced more realistic kinetics, which also allows a more detailed analysis of the soot emission mechanisms. This demonstrates the gain in accuracy obtained with improved reduced kinetics, and validates the methodology to build such schemes.

Keywords: LES, detailed modelling, soot, LST, JetA-1, surrogate, multi-component

1. INTRODUCTION

Soot particles have been proven to play a part in both climate change and public health issues. Emitted at high altitude by aircraft engines in cruise, soot particles play a negative role in the radiative forcing of the atmosphere through the promotion of contrails and contrail-induced cirrus [1]. On the ground, soot particles emitted by aircraft during taxi, landing and take-off have an adverse effect on human health after inhalation in the lungs, promoting respiratory diseases. It is important to note that these impacts are strongly dependent on the size and shape of the soot particles, which must be therefore well characterized.

As a consequence, regulations on soot particles emission become more and more stringent, pushing aircraft engine manufacturers towards new solutions for the combustor technology or the fuel. To support such developments, numerical simulation, and in particular Large-Eddy Simulation (LES), is an essential tool, allowing to understand the physics and to test new concepts in a fast and cost-effective way. However the numerical prediction of soot emission in aeronautical gas turbines is still a major challenge [2]. In particular, achieving accurate modeling of soot Particles Size Density Function (PSDF) needed to estimate their impact, is even more difficult as it involves the resolution of the formation, growth and aging of the particles alongside a comprehensive modeling of the combustion process under high pressure and temperature and at high Reynolds numbers.

Various approaches have been developed to simulate the evolution of a population of particles in a turbulent flow, which may be gathered in two categories: (i) Eulerian approaches solving for continuous functions describing the population (e.g., number density, soot mass fraction, or probability density functions) and discretized on the grid, ranging from simple semi-empirical methods such as 2-equations models to more advanced methods like the Method of Moments (MOM) and the Discrete Sectional Method (DSM) [3, 4] and (ii) Lagrangian approaches tracking each particle trajectory and evolution, either in a statistical Monte-Carlo-based formulation [5] or in a physical formulation such as the Lagrangian Soot Tracking (LST) method which proved to give accurate results for complex turbulent JetA-1/air spray flames [6]. A major difficulty with Eulerian approaches is the prediction of the particle size distribution: by construction 2-equations models do not describe the particle size, while MOM recovers it at the

*Corresponding author: riber@cerfacs.fr

expense of further assumptions and mathematical reconstruction efforts, DSM multiplies the number of variables by the number of sections discretizing the size distribution and introduces additional modeling terms. Therefore both MOM and DSM require important modeling efforts and become rapidly very computationally expensive for soot prediction in realistic burners. On the contrary, Lagrangian approaches give direct access to the size distribution at no extra cost, provided that a sufficient number or particles is computed to ensure statistical convergence. For these reasons the LST method is chosen in the present work.

The formation of soot particles results from complex heterogeneous chemical processes which occur both in gaseous and solid phases. The very first step is linked to the presence of large Polycyclic Aromatic Hydrocarbons (PAH) such as pyrene (A4) which aggregate to form the first, very small size particles [7]. These PAH molecules are barely present in the fuel and are a product of locally rich combustion where unburnt hydrocarbon chunks grow along an iterative process, well described by the HACA mechanism [8]. Then the interactions between the nascent solid soot particles and with the surrounding gas both drive their evolution through collisional phenomena, either in terms of amount (addition of mass from the gas) or particle size (formation of large aggregates by cluster aggregation).

A first modeling challenge thus lies in the description of hydrocarbon growth towards PAH under various conditions. Detailed and validated chemical kinetics exist [9–11] which proved to efficiently and accurately predict this growth, however at the cost of the inclusion of numerous intermediate species. In addition the transition toward zero-carbon emission introduces new fuels which must be taken into account in the modeling for future engine concepts. As of today, kinetics for both fuel oxidation and soot formation remain simple for simulation cost purposes at the expense of accuracy.

Regardless of the method chosen for the soot population, the objective of this work is therefore to propose a methodology to build kinetic mechanisms suitable for the LES prediction of soot emission of aeronautical engines. The kinetic mechanism shall be sufficiently compact to be computationally affordable yet as much accurate as possible. It must also include fuel effects on both the turbulent flame and the soot formation. This work thus aims at combining both fuel and soot kinetic modeling strategies in order to obtain an accurate modeling of sooting flames burning any complex fuel, while being affordable in LES of realistic aeronautical burners.

2. CONSTRUCTION OF A SEMI-DETAILED KINETIC MECHANISM

The following mostly focuses on the selection and reduction of a detailed kinetic scheme, able to predict both the combustion of a jet fuel surrogate and the subsequent soot emissions.

2.1 Workflow

The workflow is threefold and divides as follows:

1. Available and state-of-the-art detailed kinetic mechanisms are tested over several carefully chosen canonical 1D sooting flames involving both premixed and diffusion flames. The best suited mechanism is chosen based on its accuracy on soot population prediction as well as major flame properties. This selection step is performed on ethylene flames because ethylene is a simple fuel which combustion properties are well known and accurate experimental data regarding sooting ethylene flame is widely available in the literature. It thus enables to focus on the performance of the kinetic mechanism PAH growth model coupled with the chosen soot model with no uncertainties on experimental data as well as fuel and combustion modeling. While the contribution of additional pathways from aromatic compounds contained in realistic fuels to PAH is lost in the process, this step enables for the selection of mechanisms that accurately predict growth from small pyrolysis products to PAH, which remains a major contributor to soot precursors in realistic fuels.

2. Several fuel (here JetA-1) surrogates are tested with the selected mechanism, ranging from simple mono-component surrogates to larger multi-component blends involving up to 10 molecules. The best surrogate is chosen as a compromise between the accuracy of the prediction of the soot population, combustion properties and simplicity. Indeed, the efficiency of the next step inherently depends on the simplicity of the fuel surrogate. It is however possible for the chosen mechanism to lack additional pathways from large fuel compounds to PAH which would result in an underestimation of soot volume fraction for any of the tested surrogates. Let this situation happen, one would need to get back to step 1. Both steps can be performed simultaneously to avoid such issues.

3. Eventually, the selected kinetic mechanism is reduced for the chosen fuel surrogate combustion with the in-house code ARCANE [12], by minimizing the number of species while controling errors on both soot yield and flame properties on several target cases.

The aforementioned steps require an efficient tool to compute a large number of 1D canonical sooting flames at a reasonable cost. This was achieved thanks to the implementation of a DSM model in the open source software Cantera, taking advantage of the simplicity and relatively short return time of its one-dimensional solver. The resulting code, Cantera-soot, is described in the next section.

2.2 Cantera-soot

The DSM algorithm implemented in Cantera is widely inspired by the work of Rodrigues et al. [4] and is described below.

2.2.1 Governing equations of the DSM. The soot volume fraction distribution $q(v)$, with v the particle volume, being assumed constant in each section, only one moment is solved, namely the total volume fraction $M_{1,k}$ of section k, defined as:

$$M_{1,k} = \int_0^{\Delta v_k} q(v)dv = q_k \Delta v_k \tag{1}$$

where $\Delta v_k = v_k^{max} - v_k^{min}$ is the volume interval of section k and q_k its constant volume fraction distribution. The advection-diffusion equation for this moment, obtained from the Population Balance Equation (PBE), is expressed as:

$$\frac{\partial M_{1,k}}{\partial t} + \boldsymbol{\nabla} \cdot \left((\vec{u} + \vec{v_T}) M_{1,k} \right) = \boldsymbol{\nabla} \cdot \left(D_{s,k} \boldsymbol{\nabla} M_{1,k} \right) + \dot{M}_{1,k} \quad (2)$$

with $\vec{u}$ the velocity, $D_{s,k}$ the diffusion coefficient computed using Einstein's relation $D_s = k_B T / f$ and the Stokes-Millikan equation for the friction factor f [13]. The thermophoretic velocity $\vec{v_T}$ is computed in the free-molecular regime assumption following Waldmann and Schmitt [14] (ν is the gas kinematic viscosity):

$$\vec{v_T} = - \underbrace{\frac{3}{4(1 + \pi\alpha/8)}}_{\approx 0.554} \nu \frac{\boldsymbol{\nabla} T}{T} \quad (3)$$

The advection-diffusion can be rewritten in terms of the mass fraction of soot $Y_{s,k} = M_{1,k} \rho_s / \rho$ within each section k, where ρ is the fluid density and subscript s stands for soot:

$$\frac{\partial \rho Y_{s,k}}{\partial t} + \boldsymbol{\nabla} \cdot \left((\vec{u} + \vec{v_T}) \rho Y_{s,k} \right) = \boldsymbol{\nabla} \cdot \left(D_{s,k} \boldsymbol{\nabla} \left(\rho Y_{s,k} \right) \right) + \rho_s \dot{Q}_{s,k} \quad (4)$$

Soot particles density is assumed constant (ρ_s =1860 kg m^{-3}).

2.2.2 Source terms. The source term $\dot{Q}_{s,k}$ relative to each section k is the sum of all processes which impact the soot population, namely nucleation (nuc), condensation ($cond$), coagulation ($coag$), surface growth (sg) and oxidation (oxi), following:

$$\dot{Q}_{s,k} = \dot{Q}_{\text{nuc},k} + \dot{Q}_{\text{cond},k} + \dot{Q}_{\text{coag},k} + \dot{Q}_{\text{sg},k} + \dot{Q}_{\text{oxi},k} \quad (5)$$

The source term in each section k is retrieved out of the molar reaction rate $\dot{c}_{\Phi,i}$ relative to each process Φ in each section i:

$$\dot{Q}_{\Phi,k} = N_A \sum_{i=1}^{N_{\text{sections}}} V_{\Phi,ik} \, \dot{c}_{\Phi,i}, \; \Phi = nuc, cond, coag, sg, oxi \quad (6)$$

where $V_{\Phi,ik}$ is the volume added to section k by process Φ occurring in section i.

Soot inception In the implemented model, the formation of nascent soot particles is assumed to start with an irreversible two-step process (dimerization) involving the formation of a dimer by the binding of two identical PAHs:

$$\text{PAH} + \text{PAH} \longrightarrow \text{DIMER} \quad (R1)$$

The dimerization rate is computed in the free-molecular regime (due to the relatively small size of the involved PAH):

$$\begin{cases} \dot{c}_{\text{dim}} & = k_{\text{dim}} [\text{PAH}]^2 \\ k_{\text{dim}} & = \gamma_{\text{PAH}} N_A \beta_{\text{dim}} \\ \beta_{\text{dim}} & = d_{\text{PAH}}^2 \sqrt{\dfrac{4\pi k_B T}{m_{\text{PAH}}}} \end{cases} \quad (7)$$

where m_{PAH} is the PAH mass, k_B is Boltzmann constant and T the temperature. $\gamma_{\text{PAH}} = C_N W_{PAH}^4$, $C_N = 1.5 \times 10^{-11}$ mol^4 g^{-4} is a sticking coefficient which reflects that larger PAHs form more stable dimers [15] with W_{PAH} the PAH molecular weight.

Dimerization is then followed by the nucleation process which corresponds to the stacking of two dimers [8] in the same flow / collision regime:

$$\text{DIMER} + \text{DIMER} \longrightarrow \text{SOOT} \quad (R2)$$

$$\begin{cases} \dot{c}_{\text{nuc}} & = k_{\text{nuc}} [\text{DIMER}]^2 \\ k_{\text{nuc}} & = \varepsilon_{\text{nuc}} N_A \beta_{\text{nuc}} \\ \beta_{\text{nuc}} & = d_{\text{DIMER}}^2 \sqrt{\dfrac{4\pi k_B T}{m_{\text{DIMER}}}} \end{cases} \quad (8)$$

where β is the collision kernel and $\varepsilon_{\text{nuc}} = 1.3$ is an amplification factor which accounts for Van der Waals interactions [16].

Condensation Condensation corresponds to the stacking of a dimer at the surface of an existing soot particle, increasing its size:

$$\text{DIMER} + \text{SOOT} \longrightarrow \text{SOOT}^+ \quad (R3)$$

It is also assumed to occur in the free-molecular regime because of the relatively small size of the dimers:

$$\begin{cases} \dot{c}_{\text{cond}} & = k_{\text{cond}} [\text{DIMER}] [\text{SOOT}] \\ k_{\text{cond}} & = \varepsilon_{\text{cond}} N_A \beta_{\text{cond}} \\ \beta_{\text{cond}} & = \sigma_{\text{cond}} \sqrt{\dfrac{8 k_B T}{\pi m_{\text{cond}}}} \end{cases} \quad (9)$$

with σ_{cond}, m_{cond} respectively the dimer/soot system cross-section and reduced mass and $\varepsilon_{\text{cond}} = 1.3$ the amplification factor [16].

Surface chemistry Reactions occurring at the surface of soot particles involve small gaseous compounds, contributing to growth mechanisms following the HACA-RC mechanism proposed by Mauss et al. [17] in analogy with the HACA mechanism of PAH growth. They also include oxidation by OH and O_2 molecules, for which the rate constants initially proposed by Mauss in the HACA-RC mechanisms have been corrected in this work following the meta-analysis carried by Guo et al. [18]

Surface reactions are controlled by the concentration of radical sites at the surface of the particles. It is estimated following a Quasi-Steady-State (QSS) assumption:

$$\begin{cases} [\text{C}_{\text{nC}} \cdot] & = A [\text{C}_{\text{nC}}\text{H}] \\ [\text{C}_{\text{nC}}\text{C}_2\text{H}_2 \cdot] & = (AB + C) [\text{C}_{\text{nC}}\text{H}] \\ A & = \dfrac{[\text{OH}](k_{2,f} + k_{\text{OH}}) + [\text{H}] \left(k_{1,f} + k_{5,b}(1 - \epsilon) \right)}{k_{1,b}[\text{H}_2] + k_{2,b}[\text{H}_2\text{O}] + k_{3,f}[\text{H}] + k_{4,f}[\text{H}_2]\epsilon} \\ B & = k_{4,f}[\text{H}_2] \dfrac{\epsilon}{k_{5,f}} \\ C & = k_{5,b}[\text{H}] \dfrac{\epsilon}{k_{5,f}} \\ \epsilon & = \dfrac{k_{5,f}}{k_{4,b} + k_{5,f} + k_{\text{O}_2}[\text{O}_2]} \end{cases}$$

where $\text{C}_{\text{nC}}\text{H}$ represents active sites at the soot surface and all rate constants are taken from the HACA-RC mechanism [17].

The HACA-RC surface growth mechanism sums up as:

$$\mathrm{SOOT} + \mathrm{C_2H_2} \longrightarrow \mathrm{SOOT^+} + \mathrm{H_2} \tag{R4}$$

the source term is expressed as (SI units, R is the universal gas constant):

$$\begin{cases} \dot{c}_{\mathrm{sg}} & = \frac{\mathrm{d}[\mathrm{C_nCC_2H_2}\cdot]}{\mathrm{d}t} = k_1[\mathrm{C_nC}\cdot][\mathrm{C_2H_2}] - k_2[\mathrm{C_nCC_2H_2}\cdot] \\ k_1 & = 3.5\times10^7\ \mathrm{m^3\ mol^{-1}\ s^{-1}} \\ k_2 & = 3.225\times10^8 \exp\left(\frac{-1.8165\times10^5}{RT}\right)\mathrm{s^{-1}} \end{cases} \tag{10}$$

The HACA-RC oxidation mechanism takes the form:

$$\mathrm{SOOT} + \mathrm{oxidizer} \longrightarrow \mathrm{SOOT^-} + \mathrm{products} \tag{R5}$$

$$\begin{cases} \dot{c}_{\mathrm{ox}} & = \dot{c}_{\mathrm{OH}} + \dot{c}_{\mathrm{O_2}} \\ \dot{c}_{\mathrm{OH}} & = k_{\mathrm{OH}}[\mathrm{OH}][\mathrm{C_nCH}] \\ \dot{c}_{\mathrm{O_2}} & = k_{\mathrm{O_2}}[\mathrm{O_2}]\left([\mathrm{C_nC}\cdot] + [\mathrm{C_nCC_2H_2}\cdot]\right) \\ k_{\mathrm{OH}} & = 0.1\sigma_{\mathrm{s,\,OH}}\sqrt{\frac{8k_BT}{\pi m_{\mathrm{s,\,OH}}}}\mathrm{m^3\ mol^{-1}\ s^{-1}} \\ k_{\mathrm{O_2}} & = 6.15\times10^8 T^{0.5}\exp\left(\frac{-195\times10^3}{RT}\right)\mathrm{m^3\ mol^{-1}\ s^{-1}} \end{cases} \tag{11}$$

where $m_{\mathrm{s,\,OH}}$, $\sigma_{\mathrm{s,\,OH}}$ are respectively the OH/soot system reduced mass and cross-section. The efficiency constant 0.1 is taken from [18] and all units are SI.

Aggregation Aggregation resulting from collisions between soot particles is governed by collision kernels β. Recently, simulations of aggregation using Monte-Carlo methods were carried out by Moran et al. [5] under flame-like conditions and proved great consistency with the formulae proposed by Thajudeen et al. [19]. The latter are then used in the present work.

The dimensionless coagulation kernel H is defined as a function of the diffusive Knudsen number Kn_D:

$$\begin{cases} H & = \frac{4\pi Kn_D^2 + 25.836 Kn_D^3 + \varepsilon_{\mathrm{coag}}\sqrt{8\pi}11.211 Kn_D^4}{1 + 3.502 Kn_D + 7.211 Kn_D^2 + 11.211 Kn_D^3} \\ Kn_D & = \frac{\sqrt{k_B T m_{ij}}\pi r_{S,ij}}{f_{ij} PA_{ij}} \end{cases} \tag{12}$$

where $f_{ij}, m_{ij}, r_{S,ij}$ and PA_{ij} respectively correspond to the (i,j) colliding system reduced friction factor, mass, combined Smoluchowski radius and orientationally-averaged projected area as defined by the same authors. $\varepsilon_{\mathrm{coag}} = 1.3$ corresponds to an amplification factor due to Van der Waals interactions in the ballistic regime ($Kn_D \gg 1$) [16]. The collision kernel is then estimated from the dimensionless kernel H following:

$$\beta_{ij} = \frac{H f_{ij} PA_{ij}}{m_{ij}\pi^2 r_{S,ij}} \tag{13}$$

Eventually, the mass transfer between soot sections due to aggregation is expressed as in the classical DSM formalism following the Smoluchowski equation.

2.2.3 Radiation. Radiation is accounted for in an optically thin assumption using Rayleigh's theory. The radiative power of the soot population P_s^R is computed as:

$$P^R_{\mathrm{soot}} = -4\sigma\kappa_{Pl,\mathrm{soot}}T^4, \text{ with } \kappa_{Pl,\mathrm{soot}}(T) = 3.83\frac{C_0 f_V T}{C_2} \tag{14}$$

with:

$$\begin{cases} C_0 & = \frac{36\pi ab}{\left(a^2 - b^2 + 2\right) + 4a^2b^2} \\ C_2 & = \frac{hc}{k_B} \end{cases} \tag{15}$$

where h is Planck constant, c the speed of light and $m = a - ib$ ($a = 1.59$, $b = 0.56$, following Smyth and Shaddix) is the refractive index of soot.

2.3 Gaseous kinetic mechanism

Four detailed mechanisms – of various size and with various largest PAH, i.e., largest soot precursor – are tested. From the most compact to the most expensive, they are listed below:

- The BISETTI mechanism [20] consists of 47 species including naphtalene (A2) as the largest PAH and chosen soot precursor. It was tailored for ethylene sooting flames and previously used in LST simulations [6],
- The KM2 mechanism [10] consists of 202 species and includes large PAHs, i.e., 7 soot precursors ranging from pyrene (A4) to coronene (A7) (A4, chrysene, benzo-a-pyrene, benzo-e-pyrene, perylene, benzo-ghi-perylene, A7) [15]. Rodrigues et al.[4] successfully used this mechanism to perform LES of ethylene sooting flames.
- The NARAYANASWAMY mechanism [9] consists of 362 species including large-size molecules, either fuels, or PAHs up to cyclopenta-pyrene (A4R5), i.e., 5 soot precursors larger than anthracene (A3) (A3, A2R5C2H, fluoranthene, A3R5, A4, A4R5) available for the multi-PAH dimerization proposed by Blanquart et al. [15].
- The CRECK mechanism [11] is a state-of-the-art mechanism which allows detailed modeling of combustion of large-size fuels and includes PAHs up to A4 (chosen as single soot precursor). While it natively includes soot modeling capabilities using a kinetic approach which proved great capabilities on canonical ethylene flames [21], the soot reactions were removed from the mechanism to be used with DSM and LST models. The cropped CRECK mechanism finally contains 363 species.

The soot prediction capabilities of these four mechanisms coupled with the previously introduced DSM soot model have been challenged against two canonical quasi-1D flames extracted from the 4th and 5th International Sooting Flame (ISF) workshop databases. The ISF4-premixed flame 6 (ISF4-6) is a Burner Strained Stabilized (BSS) premixed flat flame that has been widely studied both experimentally [22] and numerically [21] with great consistency of the results. The ISF5 counterflow diffusion flame 1 (ISF5-CF1) has been thoroughly experimentally

studied by Gleason et al. [23] at different pressures, which will also help to assess the mechanisms pressure dependence. Both flames are fed with ethylene, which has a well-known combustion model, allowing to focus on the soot model.

2.3.1 BSS premixed flat flame (ISF4-6 case). The flame corresponds to a premixed mixture of 16.3% C_2H_4, 23.7% O_2, 60.0% Ar ($\Phi = 2.07$) at 473 K, 1 atm and injected with a velocity of 14 cm s^{-1}. The impinged plate (i.e. stagnation plane) height and temperature are varied as shown in table 1 and are used as boundary conditions at the side opposite to injection.

H_p $[mm]$	4	4.5	5.5	6	7
T_p $[K]$	500	499	497	495	492
H_p $[mm]$	8	10	12	15	20
T_p $[K]$	490	488.7	486	483	552

TABLE 1: ISF4-6 BSS case. Impinged plate height & temperature

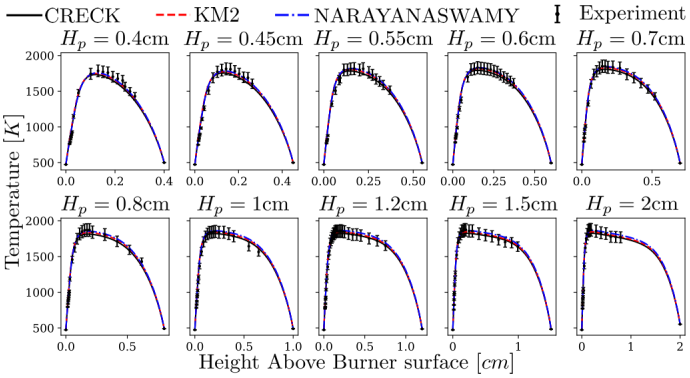

FIGURE 1: ISF4-6 BSS premixed flame. Temperature along flame centerline for varying plate height.

The 10 sooting flame cases of table 1 have been computed with Cantera-soot using 50 soot sections, with each of the above-listed mechanisms except for BISETTI which does not include argon. As displayed in fig. 1, all of the studied mechanisms accurately represent the combustion. Results in terms of soot volume fraction and particle number density at the stagnation plane are presented on fig. 2. The CRECK mechanism accurately estimates both quantities at all plate heights, with only a slight overestimation of the number density at intermediate heights, meaning too small predicted soot particles in this range. The peak of number density is however well predicted, indicating a good modeling of the soot particle evolution. The KM2 mechanism underestimates the soot amount and both the increase and decrease rates of the number density leading to a shift of the peak towards larger height. This corresponds to an underproduction of very small particles, leading first to a less dense soot population, itself responsible later for fewer particle collisions which prevents to form large aggregates. Finally, the NARAYANASWAMY mechanism dramatically underestimates the soot production, both in mass and number. To further evaluate the kinetic mechanisms, the Particle Size Distribution Function (PSDF) is compared with the measurements in fig. 3. Results confirm the accurate behavior of the CRECK mechanism: for small plate heights (H_p below 4.5mm)

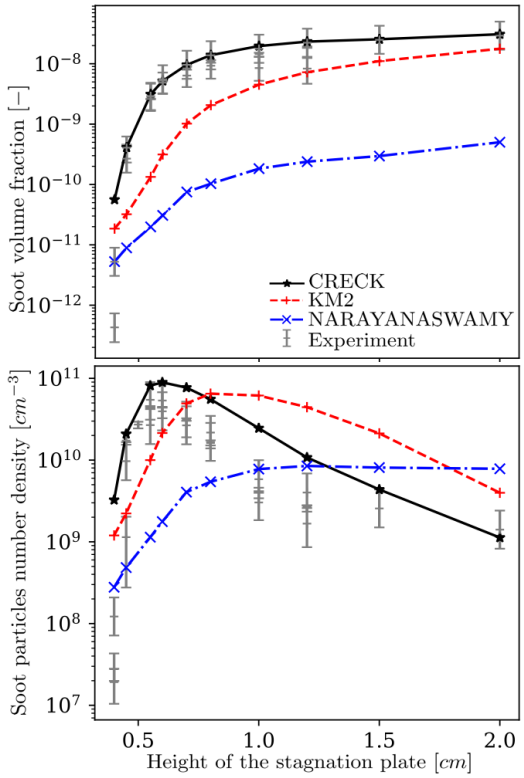

FIGURE 2: ISF4-6 BSS premixed flame. Volume fraction (top) and number density (bottom) of soot particles larger than 2nm. Cantera-soot computations (lines) vs. measurements (symbols). Simulations are shifted 2mm upstream following Saggese et al. [21]

the particle size distribution remains uni-modal, corresponding to a nucleating flame. For intermediate H_p (between 5.5 and 12mm) aggregation appears, consuming intermediate size particles to form larger ones, therefore building a second mode and pushing the PSDF towards larger particle sizes. While the prediction of this intermediate phase is not perfect, it is fairly well recovered by the CRECK mechanism. Eventually at the largest separation distances (H_p above 15mm), particles are mostly composed of large aggregates and small nucleating particles – which are still spuriously predicted by the simulation as a result of a continuous nucleation process – are absent from the measurements. With the two other mechanisms, the occurrence and intensity of the aggregation process is clearly mispredicted, leading to overall too small particles.

2.3.2 Counterflow diffusion flame (ISF5-CF1 case). The setup experimentally studied by Gleason et al. [23] consists of two facing nozzles of diameter 6.35 mm separated by 8 mm. The fuel stream is composed of 26.5% C_2H_4 and 73.5% N_2 (mol.) at 298 K ejected at 20.1 cm s^{-1} while the oxidizer stream is composed of 18.3% O_2 and 81.7% N_2 (mol.) at 323 K, 19.9 cm s^{-1}. Simulation results obtained with the four mechanisms are compared with measurements at 1 and 4 atm. As displayed in fig. 4, all studied mechanisms accurately predict the flame temperature. Species of interest when it comes to PAH growth are represented in fig. 5. It appears that all mechanisms accurately predict C_2H_2 as well as benzene (A1) and A2 (the soot precursor used for the

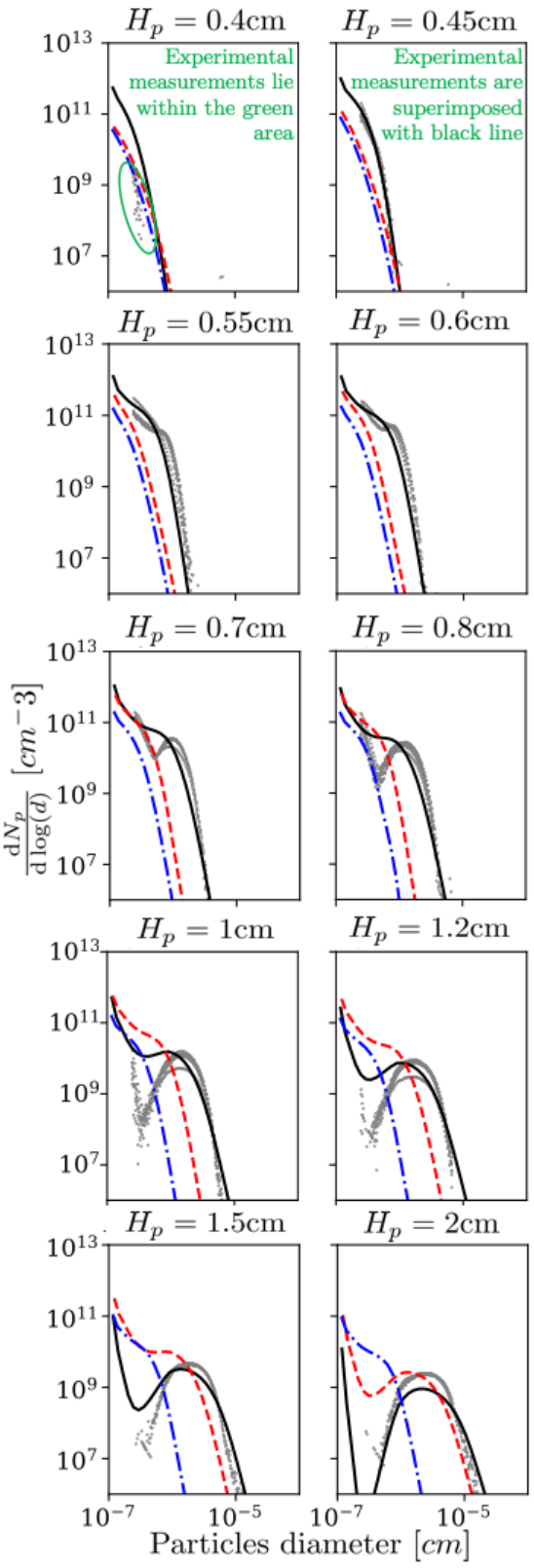

FIGURE 3: ISF4-6 BSS premixed flame. Particle Size Distribution Function (PSDF) 2mm upstream the stagnation plane for different separation heights. Cantera-soot computations (lines) vs. measurements (gray symbols). Same legend as in fig. 2.

BISETTI mechanism). A4 is accurately predicted by the KM2 mechanisms while the NARAYNASWAMY mechanism underestimates its production. The CRECK mechanism on the other hand tends to overestimate its production.

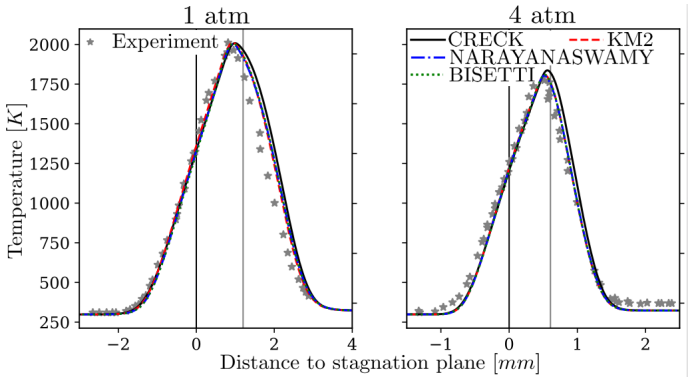

FIGURE 4: ISF5-CF1 counterflow diffusion flame. Temperature along flame centerline at atmospheric (left) and moderately elevated (right) pressure. Vertical lines indicate the stagnation plane (black, x = 0) and the stoichiometric mixture fraction (grey).

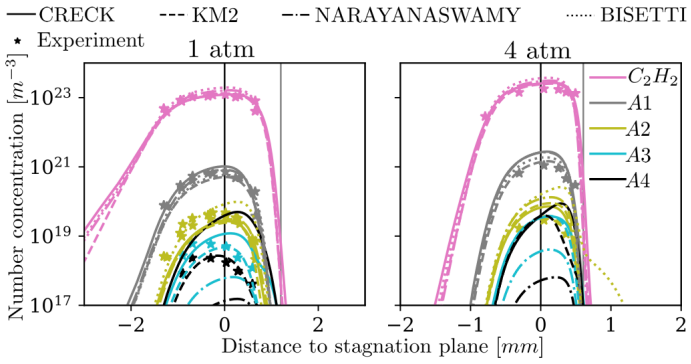

FIGURE 5: ISF5-CF1 counterflow diffusion flame. Species concentration along flame centerline at atmospheric (left) and moderately elevated (right) pressure.

Figure 6 shows that both CRECK and BISETTI mechanisms well predict the soot volume fraction at both pressures while KM2 and NARAYANASWAMY mechanisms strongly underestimate the soot production, similarly to what was observed in the previous premixed flame. Insights given in fig. 5 show that the underestimation of soot particles with the KM2 mechanism could rather be linked to an underestimation of soot nucleation and dimers condensation than an underestimation of soot precursors by the gaseous mechanism. The soot model could thus be improved in future works. The particle number density however is underestimated by all mechanisms by at least one order of magnitude. This discrepancy is still to be explained, but a possible and partial cause may be due to the mathematical reconstruction of the number density based on scattering coefficients used in the experiment.

Overall and out of all studied mechanisms, the CRECK mechanism seems to perform best and is kept as a reference in the following.

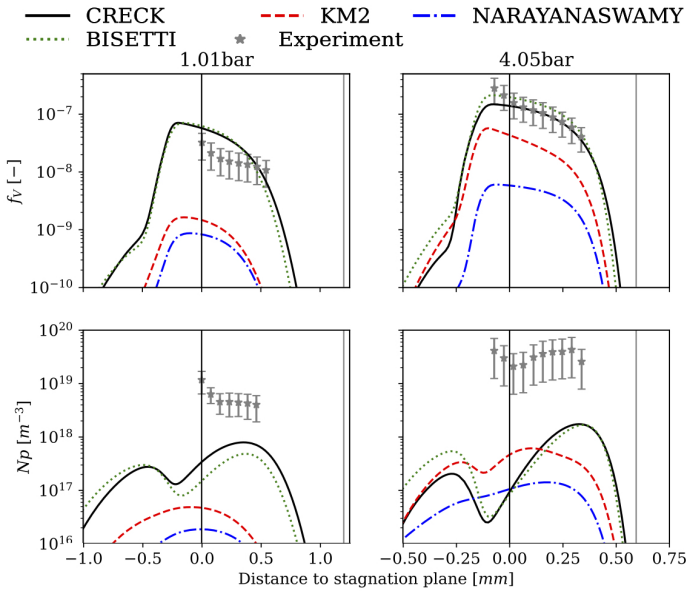

FIGURE 6: ISF5-CF1 counterflow diffusion flame. Soot volume fraction (top) and particles number density (bottom) at atmospheric (left) and moderately elevated (right) pressures. Cantera-soot computations (lines) vs. measurements (symbols).

2.4 Fuel surrogate

Name	Composition
n-decane	100% n-decane
Aachen [24]	80% n-decane, 20% methyl-cyclohexane
Humer C [25]	60% n-dodecane 20% methyl-cyclohexane, 20% xylene
MURI2 [26]	40% n-dodecane, 30% i-octane 23% n-propylbenzene, 7% trimethylbenzene
Hex12 [27]	30% n-decane, 27% decalin 13% tetralin, 12% n-dodecane, 3% n-octane
POLIMI [28]	3 to 10 components Detailed in [28]

TABLE 2: Composition of Jet-A1 surrogates.

Aeronautical fuels are complex blends of numerous molecules, and must be modeled as so-called surrogates. The number, the nature and the amount of surrogate compounds are critical to accurately represent fuel effects on the flame and pollutant emissions. In this section, different Jet-A1 surrogates extracted from the literature and ranging from simple mono-component surrogates (n-decane) to large complex surrogates involving up to 10 components (listed in table 2) coupled with the CRECK mechanism are challenged against measurements on laminar flame speed, auto-ignition delay time and soot volume fraction to assess their ability to model JetA-1 combustion and soot production. Experimental flame speed measurements were carried by Kumar et al. [29] and Hui et al. [30] at 1 and 3 atm. Results are represented in fig. 7. It appears that n-decane overestimates the flame speed hence the need for a more complex description when it comes to combustion modeling. All of the multi-component surrogates perform reasonably well, with larger surrogates more accurate at elevated pressure while no clear pattern is visible at atmospheric pressure. Auto-ignition delay times were measured by Mullins et al. [31] and Freeman and Lefebvre [32]. Results are represented in fig. 8 and exhibit accurate predictions for all of the tested surrogates except the POLIMI-3 species and POLIMI-6 species, with larger surrogates behaving slightly better for the highest temperatures.

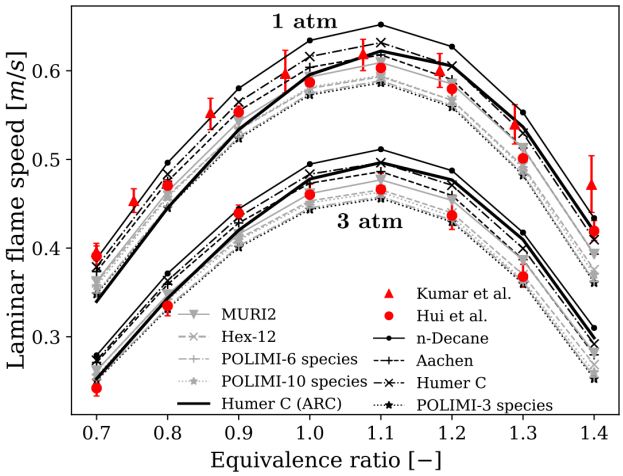

FIGURE 7: Computed Jet-A1 laminar flame speed at fresh gas temperature 400 K and pressure 1 to 3 atm for varying surrogates. The reduced ARC_MULTI_LST mechanism derived in section 2.5 is represented for validation purposes.

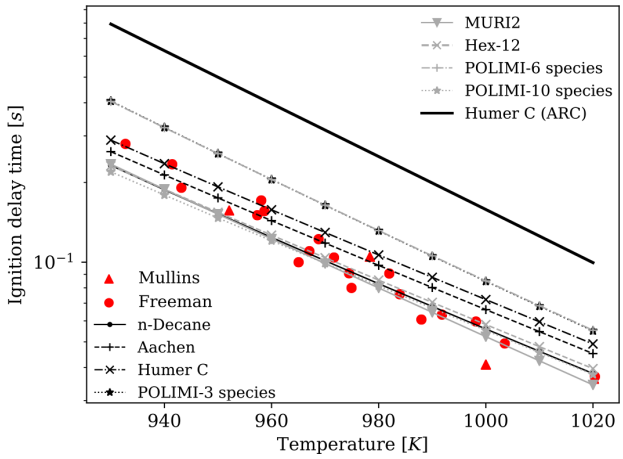

FIGURE 8: Jet-A1 auto-ignition delay time at 1 atm for various surrogates. The reduced ARC_MULTI_LST mechanism derived in section 2.5 is represented for validation purposes.

As experiments on canonical sooting flames with jet fuels are much scarcer than with ethylene, only one documented enough case could be found and used as reference. The reference flame, proposed by Xue et al. [33], consists of two facing converging nozzles of diameter 10 mm and separated by 11 mm, operating at atmospheric pressure. The fuel and oxidizer streams are respectively composed of 10% Jet-A1 and 40% O_2, both diluted in N_2 at 473 K and injected at equal velocity leading to a strain rate of 200 s^{-1}. Soot volume fraction is observed along the centerline and results are shown in fig. 9.

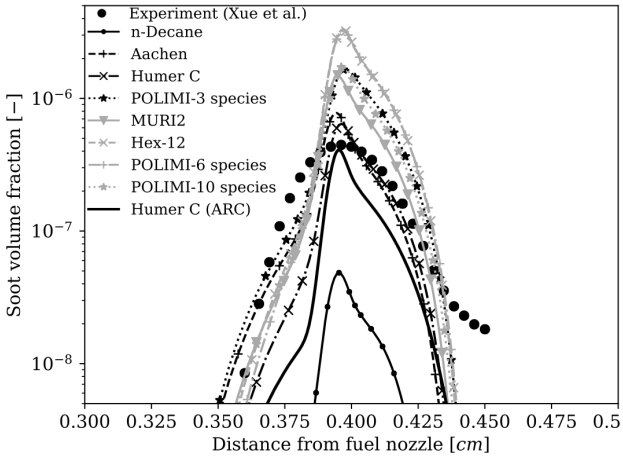

FIGURE 9: Jet-A1 counterflow diffusion flame. Soot volume fraction along the centerline, computed with various surrogates (lines) and the CRECK mechanism, compared with experiment (markers).

As it can be seen from fig. 9, and as could be expected, the simple mono-component surrogate dramatically underestimates the soot volume fraction. But more surprisingly the most complex surrogates do not give the best results. It appears that the 3-components surrogates overall lead to the best prediction of the soot volume fraction. The Humer C surrogate is finally kept in the following since it remains simple enough and performs reasonably well in terms of laminar flame speed, auto-ignition delay time and soot estimation. Moreover it was recently validated in jet fuel spray flames [34].

Freely propagating 1D flames					
P [bar]	T [K]	Φ [-]	S_L, $\int$ HRR	$Y_{A4,max}$	$Y_{A4,end}$
4.338	300, 700	0.6 - 1.5	15%	-	-
		2.0	15%	50%	-
		2.5	15%	30%	35%
		3.0	15%	30%	30%

0D isochoric reactor			
P [bar]	T [K]	Φ [-]	Ignition delay time
4.338	800	0.5 - 3.0	99.9%
	1500		9.9%

TABLE 3: Summary of test cases with associated tolerances for chemistry reduction.

2.5 Reduction of the kinetic mechanism

The CRECK detailed mechanism is unfortunately far too large to be used in LES of a 3D complex geometry turbulent flame. In addition it involves numerous radical species with very short timescales, leading to strong numerical stiffness. To overcome this difficulty, the mechanism is analytically reduced with the code ARCANE [12] using a Direct Relation Graph with Error Propagation (DRG-EP) methodology to detect and remove unnecessary species and reactions given reference cases and target errors, which are summed up in table 3. The test cases are computed with the Humer C surrogate and the target quantities include PAHs concentrations. The resulting skeletal mechanism consists of 67 species and 448 reversible reactions, which makes it much more compact yet still too heavy to be used in LES. An ultimate reduction step is then applied, based on the QSS assumption for the fastest species (ranked using the Level Of Importance

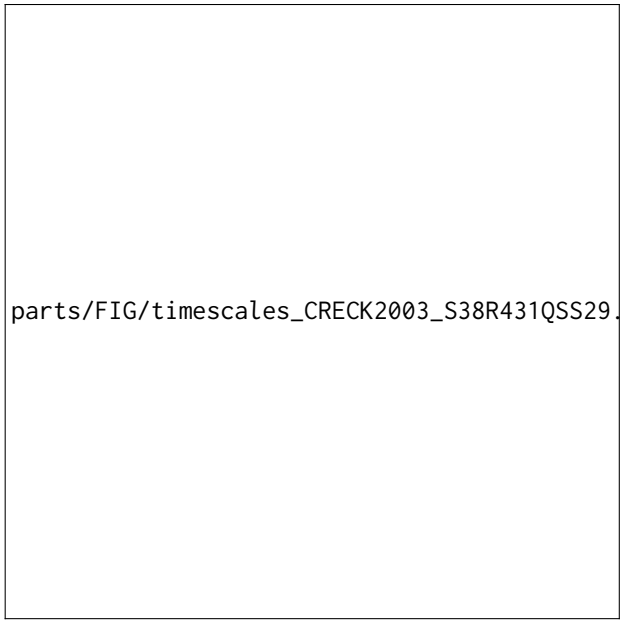

FIGURE 10: Species timescales of the semi-detailed ARC_MULTI_LST kinetic mechanism obtained in a premixed flat flame at 4 atm and stoichiometric conditions. The red line corresponds to the time step at which the LES is expected to run.

formalism): their concentration is assumed constant and may be analytically retrieved from the other species concentrations. Thanks to the QSS assumption, 29 stiff species are removed from the skeletal mechanism, leading to a final semi-detailed mechanism containing 38 species and 431 reversible reactions, denoted ARC_MULTI_LST. Its accuracy is challenged against its detailed counterpart in figs. 7 to 9. It appears that laminar flame speed is accurately recovered and lies within the range of all the tested surrogates. Auto-ignition delay time is however widely overestimated which comes from the extremely slack tolerances applied on this criterion during the chemistryreduction since ignition is not the target of the study. Eventually, while soot yield decreases because of the removal of minor PAH growth pathways during the reduction process, it remains accurate enough for the targeted applications. Eventually, the timescales of the remaining species are represented in fig. 10: the smallest ones are in the range of the time step used for an explicit-in-time flow integration.

3. APPLICATION : THE HERON-RQL CONFIGURATION

The HERON burner is a Rich-Quench-Lean configuration was thoroughly studied at CORIA by Perrier et al. [35], with a focus on the measurement of soot production in the rich zone. For the computed working point (PF2 in [35]), the burner operates at (700 K, 4.5 bar) and is equipped with an aerodynamic injector provided by Safran Aircraft Engines. This test rig is intended to study combustion in conditions representative of an aeronautical jet engine. Similarly to the experimental study, in the following the focus is made on the modeling of the rich zone of the RQL burner, where soot is mostly assumed to form.

3.1 Computational domain and mesh

The computational domain is represented in fig. 11. It includes a plenum, the injection system (hidden for confidentiality reasons), the combustion chamber and the exit nozzle. Note also the presence of a sampling probe, which is accounted for in the geometry in view of its size and location.

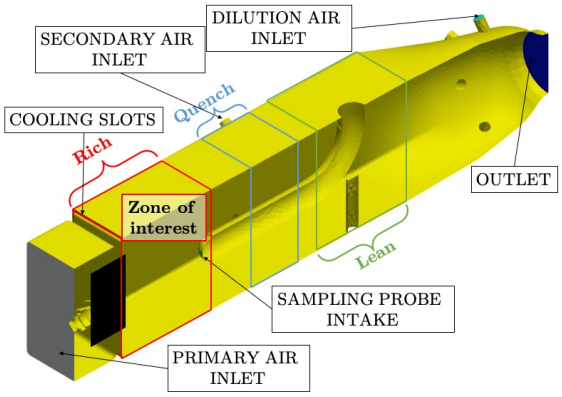

FIGURE 11: HERON-RQL : Computational domain. The injection system is hidden for confidentiality reasons.

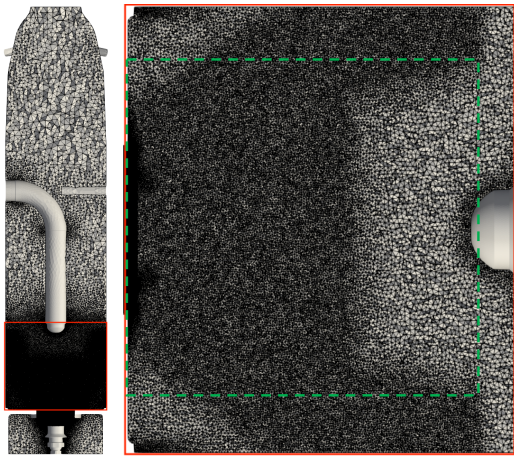

FIGURE 12: HERON-RQL : computational mesh. Left: global view. Right: zoom on the rich reactive zone. The injection system is hidden for confidentiality reasons. The visualization window is represented in green dashes.

The computational mesh represented in fig. 12 consists of 40M elements, mostly located in the injection system and the flame zone (ensuring at least 10 elements in each vane height, $y^+ < 100$ and cells narrower than 0.5 mm in the flame zone).

3.2 LES modeling strategy

The discretized formulation of the compressible reactive Navier-Stokes equations is solved with the massively parallel LES solver AVBP developed at CERFACS [36]. Explicit time-stepping is done by a four-steps Runge-Kutta scheme while convective fluxes are computed by the second-order finite volumes Lax-Wendroff scheme. Boundary conditions are handled in a non-reflective NSCBC formalism while near-wall flow is modeled with a logarithmic wall-law. Subgrid-scale terms are calculated using the SIGMA model . Radiation is neglected.

The chemical solver uses an exponential time-integration of the source terms [37] and a constant sub-cycling set to 45 to handle the stiffness of the combustion of droplets crossing the flame-front. Premixed flames are artificially thickened using the Thickened Flame (TF) approach while diffusion flames are left as is [38]. Liquid fuel is injected following the FIM-UR model for pressure-swirl atomizers and a droplet-size Rosin-Rammler distribution which parameters were provided by Safran Aircraft Engines. Multi-component evaporation is handled according to Shastry et al. [34]. The LST approach implemented in AVBP is used to model the soot population [6], the variations in soot production caused by the switch bewteen DSM and LST models is expected to be marginal since the consistency between both methods has already been validated in [6]. Due to their small size, soot particles are assumed to behave like flow tracers (both diffusion and thermophoresis transports are neglected). Because soot transport is insensitive to acoustics, the soot solver is over-cycled to reach a time step about 10 times the time step of the compressible flow solver. Finally, using the parcel concept where a numerical particle represents a set of physical particles having similar properties, the number of numerical particles per cell is kept below 10.

4. RESULTS & DISCUSSION

Two simulations of the HERON-RQL configuration have been performed and are compared to the measurements. They differ by the kinetics employed: the ARC_MULTI_LST case employs the kinetics derived in Sections 2.4 & 2.5 with A4 as soot precursor, while the ARC_MONO_LST case corresponds to a previous in-house approach developed for mono-component fuels, based on the HyChem paradigm for fuel pyrolysis and the BISETTI mechanism for both combustion and PAH growth up the corresponding soot precursor : A2 [6].

Cut fields of average soot volume fraction in the rich zone of the chamber is represented in fig. 13. It appears clearly that the mono-component approach barely estimates any soot production in comparison with the measurement, whereas the multi-component model proposed in this work predicts a correct amount of soot. Simulation results however show a too early soot production where the soot volume fraction is locally too high. However a similar distribution pattern is observed in fig. 14 between the multi-component simulation and the experiment, with soot presence in both the Outer Shear Layer (OSL) and the Inner Recirculation Zone (IRZ), while the region between the two zones exhibiting a low amount of soot particles corresponds to the flame. Accounting for the multi-component nature of real fuels therefore seems to be critical for an accurate description of soot formation and evolution under aeronautical flame conditions. The good agreement with measurements hence authorizes a thorough analysis to understand the soot production mechanisms, as presented below.

To further analyse the mechanisms of soot production in such burner, fig. 14 shows cut fields of various soot properties with super-imposed streamlines (top-half) and isolines of the different soot source terms. As is typical for such swirled flame, the flow

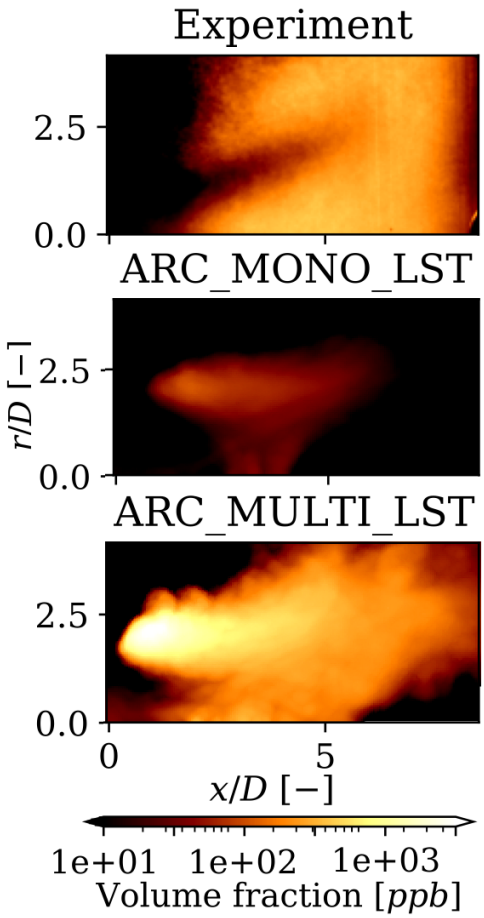

FIGURE 13: HERON-RQL: cut fields of average soot volume fraction in the rich zone. Comparison of experiment (top), LES with ARC_MONO_LST (middle) and LES with ARC_MULTI_LST (bottom). Results are represented in logarithmic scale.

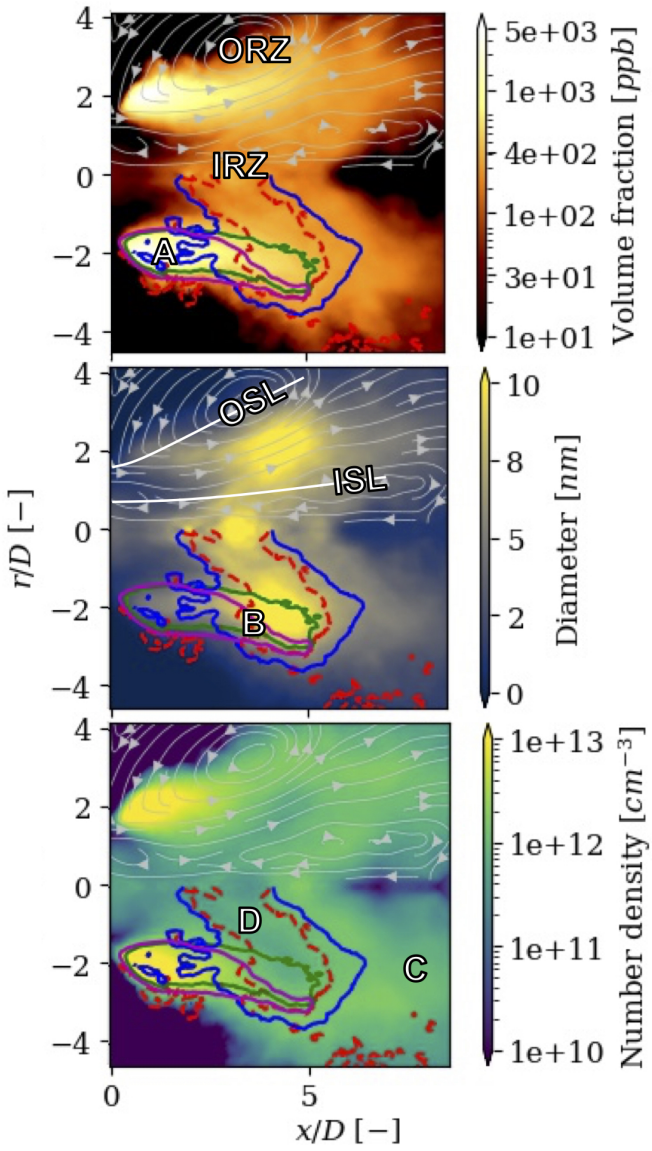

FIGURE 14: HERON-RQL: cut fields of average fields of soot volume fraction (top), particles nuclei diameter (middle) and particles number density (bottom), superimposed with isolines of precursor concentration (—), surface growth (—), condensation (—) & oxidation (- -). Gray arrows represent the flow stream.

structure is composed of Outer Recirculation Zones (ORZ) in the corners and one IRZ separated by a shear flow, delimited by the Outer (OSL) and Inner (ISL) Shear Layers where the flame is located. It appears from fig. 14 that soot is mostly formed inside the mean shear flow, i.e., between the OSL and ISL. Interestingly, the high soot volume fraction best correlates with condensation, while large soot diameters correlate best with surface growth and high soot number density with PAH concentration. These observations allow to draw a scenario for soot production and evolution in this flame. In the close-to-injection rich zone, evaporating fuel droplets and unburnt hydrocarbons that have crossed the flame front degrade into PAHs leading to strong soot nucleation, i.e., peak soot volume fraction and number density. This corresponds to region A in fig. 14(top) characterized with high load of small particles, as confirmed by the small particle diameter in this zone due to the nascent particles. Convected by the flow, soot particles then undergo condensation as well as surface growth in the shear flow region B fig. 14(middle) between both recirculation zones : the volume fraction remains high, while the number density decreases and the primary particles diameter increases, highlighting the maturation of soot particles towards large aggregates. Eventually, large aggregates either follow the main stream where they encounter less favorable conditions and are mostly oxidized into smaller particles (region C in fig. 14(bottom)) or get trapped in the IRZ where surface growth and oxidation compete to form a small amount of large aggregates (region D in fig. 14(bottom)).

The CPU cost of the simulations is reported in table 4 alongside its cost with a simple 2-steps chemistry that does not provide any information on soot. As expected the computational cost increases with the complexity of the chemistry, and is the same order for both reduced mechanisms. The overcost of ARC_MULTI_LST in comparison with the ARC_MONO_LST is mostly explained by an increased stiffness due to less volatile fuels leading to droplets crossing the flame front.

Performance	2S	MONO_LST	MULTI_LST
it/s/CPU	4e-3	7e-4	4e-4

TABLE 4: CPU performance for the tested soot models

5. CONCLUSIONS

Taking advantage of available and newly developed chemistry modeling and manipulation tools has allowed the development of a semi-detailed combustion and PAH growth kinetic mechanism, taking into account the fuel complexity. The mechanism could be straightforwardly plugged into the LES solver AVBP and significantly improved the soot prediction capabilities under realistic aeronautical applications. The presented methodology and workflow may be used for any fuel, detailed mechanism and application, providing useful information and thorough details about soot formation in complex flows. The mechanism remains however quite computationally intensive and further modeling efforts such as pathway lumping for both pyrolysis and PAH growth within the reduction process (*i.e.* while controling their impact on soot prediction) are under investigation to enable for further reduction of the mechanisms.

ACKNOWLEDGMENTS

This work was supported by the ANR ASTORIA project, grant ANR-18-CE05-0015 of the French Agence Nationale de Recherche. The financial support was provided by SafranTech through the project ALTERNATE (Horizon 2020 research and innovation program under the Marie Sklodowska-Curie grant agreement No. 875538). The injector geometry and the experimental data were provided by Safran Aircraft Engines through the National APLAREP program funded by the French Délégation Générale de l'Aviation Civile (DGAC). This work was performed using HPC resources from GENCI-IDRIS (Grant 2022-A0132B10157).

REFERENCES

[1] Kärcher, Bernd. "Formation and radiative forcing of contrail cirrus." *Nature Communications* Vol. 9 No. 1 (2018): p. 1824. DOI 10.1038/s41467-018-04068-0.

[2] Fiorina, Benoit, Vié, Aymeric, Franzelli, Benedetta, Darabiha, Nasser and Massot, Marc et al. "Modeling Challenges in Computing Aeronautical Combustion Chambers." *Aerospace Lab* No. 11 (2016): p. 19 pages. DOI 10.12762/2016.AL11-05.

[3] Netzell, Karl, Lehtiniemi, Harry and Mauss, Fabian. "Calculating the soot particle size distribution function in turbulent diffusion flames using a sectional method." *Proceedings of the Combustion Institute* Vol. 31 I No. 1 (2007): pp. 667–674. DOI 10.1016/j.proci.2006.08.081.

[4] Rodrigues, Pedro, Franzelli, Benedetta, Vicquelin, Ronan, Gicquel, Olivier and Darabiha, Nasser. "Coupling an LES approach and a soot sectional model for the study of sooting turbulent non-premixed flames." *Combustion and Flame* Vol. 190 (2018): pp. 477–499. DOI 10.1016/j.combustflame.2017.12.009.

[5] Morán, Jose, Yon, Jérôme, Poux, Alexandre, Corbin, Frédéric, Ouf, François-Xavier and Siméon, Andrea. "Monte Carlo Aggregation Code (MCAC) Part 2: Application to soot agglomeration, highlighting the importance of primary particles." *Journal of Colloid and Interface Science* Vol. 575 (2020): pp. 274–285. DOI 10.1016/j.jcis.2020.04.085.

[6] Gallen, Lucien, Riber, Eleonore and Cuenot, Bénédicte. "Investigation of soot formation in turbulent spray flame burning real fuel." *Combustion and Flame* (2023): p. 112621DOI 10.1016/j.combustflame.2023.112621.

[7] Andrade-Eiroa, Auréa, Leroy, Valérie, Dagaut, Philippe and Bedjanian, Yuri. "Determination of Polycyclic Aromatic Hydrocarbons in kerosene and bio-kerosene soot." *Chemosphere* Vol. 78 No. 11 (2010): pp. 1342–1349. DOI 10.1016/j.chemosphere.2010.01.005.

[8] Frenklach, Michael and Wang, Hai. "Detailed modeling of soot particle nucleation and growth." *Symposium (International) on Combustion*, Vol. 23. 1: pp. 1559–1566. 1991. DOI 10.1016/S0082-0784(06)80426-1.

[9] Narayanaswamy, Krithika, Blanquart, Guillaume and Pitsch, Heinz. "A consistent chemical mechanism for oxidation of substituted aromatic species." *Combustion and Flame* Vol. 157 No. 10 (2010): pp. 1879–1898. DOI 10.1016/j.combustflame.2010.07.009.

[10] Wang, Yu, Raj, Abhijeet and Chung, Suk Ho. "A PAH growth mechanism and synergistic effect on PAH formation in counterflow diffusion flames." *Combustion and flame* Vol. 160 No. 9 (2013): pp. 1667–1676. DOI 10.1016/j.combustflame.2013.03.013.

[11] Ranzi, Eliseo, Cavallotti, Carlo, Cuoci, Alberto, Frassoldati, Alessio, Pelucchi, Matteo and Faravelli, Tiziano. "New reaction classes in the kinetic modeling of low temperature oxidation of n-alkanes." *Combustion and Flame* Vol. 162 No. 5 (2015): pp. 1679–1691. DOI 10.1016/j.combustflame.2014.11.030.

[12] Cazères, Quentin, Pepiot, Perrine, Riber, Eleonore and Cuenot, Bénédicte. "A fully automatic procedure for the analytical reduction of chemical kinetics mechanisms for Computational Fluid Dynamics applications." *Fuel* Vol. 303 (2021): p. 121247. DOI 10.1016/j.fuel.2021.121247.

[13] Davies, Charles Norman. "Definitive equations for the fluid resistance of spheres." *Proceedings of the Physical Society* Vol. 57 No. 4 (1945): p. 259. DOI 10.1088/0959-5309/57/4/301.

[14] Waldmann, L and Schmitt, KH. "Thermophoresis and diffusiophoresis of aerosols." *Aerosol science*. Vol. 137. Academic Press New York (1966).

[15] Blanquart, Guillaume and Pitsch, Heinz. "A joint volume-surface-hydrogen multi-variate model for soot formation." Bockhorn, Henning, D'Anna, Andrea, Sarofim, Adel F. and Wang, Hai (eds.). *Combustion Generated Fine Carbonaceous Particles*. KIT Scientific Publishing (2007): pp. 437–463. DOI 10.5445/KSP/1000013744.

[16] Marchal, Caroline. "Modélisation de la formation et de l'oxydation des suies dans un moteur automobile." Ph.D. Thesis, Université d'Orléans. 2008. URL theses.hal.science/tel-00392316.

[17] Mauss, Fabian, Netzell, Karl and Lehtiniemi, Harry. "Aspects of modeling soot formation in turbulent diffusion flames." *Combustion Science and Technology* Vol. 178 No. 10-11 (2006): pp. 1871–1885. DOI 10.1080/00102200600790888.

[18] Guo, Haiqing, Anderson, Paul M and Sunderland, Peter B. "Optimized rate expressions for soot oxidation by OH and O 2." *Fuel* Vol. 172 (2016): pp. 248–252. DOI 10.1016/j.fuel.2016.01.030.

[19] Thajudeen, Thaseem, Gopalakrishnan, Ranganathan and Hogan, Christopher J. "The collision rate of nonspherical particles and aggregates for all diffusive knudsen numbers." *Aerosol Science and Technology* Vol. 46 No. 11 (2012): pp. 1174–1186. DOI 10.1080/02786826.2012.701353.

[20] Bisetti, Fabrizio, Blanquart, Guillaume, Mueller, Michael E. and Pitsch, Heinz. "On the formation and early evolution of soot in turbulent nonpremixed flames." *Combustion and Flame* Vol. 159 (2012): pp. 317–335. DOI 10.1016/j.combustflame.2011.05.021.

[21] Saggese, Chiara, Ferrario, Sara, Camacho, Joaquin, Cuoci, Alberto, Frassoldati, Alessio, Ranzi, Eliseo, Wang, Hai and Faravelli, Tiziano. "Kinetic modeling of particle size distribution of soot in a premixed burner-stabilized stagnation ethylene flame." *Combustion and Flame* Vol. 162 No. 9 (2015): pp. 3356–3369. DOI 10.1016/j.combustflame.2015.06.002.

[22] Camacho, Joaquin, Liu, Changran, Gu, Chen, Lin, He, Huang, Zhen, Tang, Quanxi, You, Xiaoqing, Saggese, Chiara, Li, Yang, Jung, Heejung, Deng, Lei, Wlokas, Irenaeus and Wang, Hai. "Mobility size and mass of nascent soot particles in a benchmark premixed ethylene flame." *Combustion and Flame* Vol. 162 No. 10 (2015): pp. 3810–3822. DOI 10.1016/j.combustflame.2015.07.018.

[23] Gleason, Kevin, Carbone, Francesco and Gomez, Alessandro. "PAHs controlling soot nucleation in 0.101—0.811MPa ethylene counterflow diffusion flames." *Combustion and Flame* Vol. 227 (2021): pp. 384–395. DOI 10.1016/j.combustflame.2021.01.015.

[24] Honnet, S., Seshadri, K., Niemann, U. and Peters, N. "A surrogate fuel for kerosene." *Proceedings of the Combustion Institute* Vol. 32 I No. 1 (2009): pp. 485–492. DOI 10.1016/j.proci.2008.06.218.

[25] Humer, Stefan, Seiser, Reinhard and Seshadri, Kalyanasundaram. "Experimental investigation of combustion of jet fuels and surrogates in nonpremixed flows." *Journal of Propulsion and Power* Vol. 27 No. 4 (2011): pp. 847–855. DOI 10.2514/1.46916.

[26] Dooley, Stephen, Won, Sang Hee, Chaos, Marcos, Heyne, Joshua, Ju, Yiguang, Dryer, Frederick L, Kumar, Kamal, Sung, Chih-Jen, Wang, Haowei, Oehlschlaeger, Matthew A et al. "A jet fuel surrogate formulated by real fuel properties." *Combustion and Flame* Vol. 157 No. 12 (2010): pp. 2333–2339. DOI 10.1016/j.combustflame.2010.07.001.

[27] Eddings, Eric G., Yan, Shihong, Ciro, William and Sarofim, Adel F. "Formulation of a surrogate for the simulation of Jet fuel pool fires." *Combustion Science and Technology* Vol. 177 No. 4 (2005): pp. 715–739. DOI 10.1080/00102200590917248.

[28] Pertesana, Simone. "Jet fuel surrogates formulation and metamodeling of fuel mixtures properties." MSc. Thesis (2021). URL hdl.handle.net/10589/179062.

[29] Kumar, Kamal, Sung, Chih-Jen and Hui, Xin. "Laminar flame speeds and extinction limits of conventional and alternative jet fuels." *Fuel* Vol. 90 No. 3 (2011): pp. 1004–1011. DOI 10.1016/j.fuel.2010.11.022.

[30] Hui, Xin and Sung, Chih-Jen. "Laminar flame speeds of transportation-relevant hydrocarbons and jet fuels at elevated temperatures and pressures." *Fuel* Vol. 109 (2013): pp. 191–200. DOI 10.1016/j.fuel.2012.12.084.

[31] Mullins, B.P. "The spontaneous combustion of fuels injected into a hot gas stream." *Symposium on Combustion and Flame, and Explosion Phenomena* Vol. 3 No. 1 (1948): pp. 704–713. DOI https://doi.org/10.1016/S1062-2896(49)80097-3.

[32] Freeman, G. and Lefebvre, A.H. "Spontaneous ignition characteristics of gaseous hydrocarbon-air mixtures." *Combustion and Flame* Vol. 58 No. 2 (1984): pp. 153–162. DOI https://doi.org/10.1016/0010-2180(84)90090-7.

[33] Xue, Xin, Hui, Xin, Singh, Pradeep and Sung, Chih Jen. "Soot formation in non-premixed counterflow flames of conventional and alternative jet fuels." *Fuel* Vol. 210 No. August (2017): pp. 343–351. DOI 10.1016/j.fuel.2017.08.079.

[34] Shastry, Varun, Cazeres, Quentin, Rochette, Bastien, Riber, Eleonore and Cuenot, Bénédicte. "Numerical study of multicomponent spray flame propagation." *Proceedings of the Combustion Institute* Vol. 38 No. 2 (2021): pp. 3201–3211. DOI 10.1016/j.proci.2020.07.090.

[35] Perrier, Aurélien, Milea, Andrei-Silviu, Caceres, Marcos, Vandel, Alexis, Godard, Gilles, Cayre, Alain, Collin-Bastiani, Félix, Cabot, Gilles and Grisch, Frédéric. "Soot Formation and Flame Characterization in a Swirl Kerosene Spray Rich Burn-Quench-Lean Burner at Elevated Pressure." *Turbo Expo: Power for Land, Sea, and Air*, Vol. 86960: p. V03BT04A048. 2023. DOI 10.1115/GT2023-103642.

[36] Gourdain, Nicolas, Gicquel, Laurent, Montagnac, Marc, Vermorel, Olivier, Gazaix, Michel, Staffelbach, Gabriel, Garcia, Marta, Boussuge, Jean-François and Poinsot, Thierry. "High performance parallel computing of flows in complex geometries: I. Methods." *Computational Science Discovery* Vol. 2 No. 1 (2009): p. 015003. DOI 10.1088/1749-4699/2/1/015003.

[37] Blanchard, Simon, Cazères, Quentin and Cuenot, Bénédicte. "Chemical modeling for methane oxy-combustion in Liquid Rocket Engines." *Acta Astronautica* Vol. 190 (2022): pp. 98–111. DOI 10.1016/j.actaastro.2021.09.039.

[38] Cuenot, Bénédicte, Shum-Kivan, Francis and Blanchard, Simon. "The thickened flame approach for non-premixed combustion: Principles and implications for turbulent combustion modeling." *Combustion and Flame* Vol. 239 (2022): p. 111702. DOI 10.1016/j.combustflame.2021.111702.